Journal of Biomolecular NMR, **24:** 41–50, 2002.
KLUWER/ESCOM

Novel projected 4D triple resonance experiments for polypeptide backbone chemical shift assignment

Youlin Xia[a,c,*], Cheryl H. Arrowsmith[a,c,**] & Thomas Szyperski[b,c,**]
[a]*Ontario Cancer Institute and Department of Medical Biophysics, The University of Toronto, Toronto, ON, Canada M5G 2M9;* [b]*Department of Chemistry, University at Buffalo, The State University of New York, Buffalo, NY 14260, U.S.A.;* [c]*The Northeast Structural Genomics Consortium*

Received 8 April 2002; Accepted 27 July 2002

Key words: automated protein NMR assignment, protein structure, reduced-dimensionality triple-resonance experiments, resolution enhancement, structural genomics

Abstract

Here we present a novel suite of projected 4D triple-resonance NMR experiments for efficient sequential assignment of polypeptide backbone chemical shifts in $^{13}C/^{15}N$ doubly labeled proteins. In the 3D HNN[CAHA] and 3D HNN(CO)[CAHA] experiments, the $^{13}C^{\alpha}$ and $^{1}H^{\alpha}$ chemical shifts evolve in a common dimension and are *simultaneously* detected in quadrature. These experiments are particularly useful for the assignment of glycine-rich polypeptide segments. Appropriate setting of the ^{1}H radiofrequency carrier allows one to place cross peaks correlating either backbone $^{15}N/^{1}H^{N}/^{13}C^{\alpha}$ or $^{15}N/^{1}H^{N}/^{1}H^{\alpha}$ chemical shifts in separate spectral regions. Hence, peak overlap is not increased when compared with the conventional 3D HNNCA and HNN(CA)HA. 3D HNN[CAHA] and 3D HNN(CO)[CAHA] are complemented by 3D reduced-dimensionality (RD) HNN COCA and HNN CACO, where $^{13}C^{\alpha}$ and $^{13}C'$ chemical shifts evolve in a common dimension. The $^{13}C^{\alpha}$ shift is detected in quadrature, which yields peak pairs encoding the $^{13}C'$ chemical shift in an in-phase splitting. This suite of four experiments promises to be of value for automated high-throughput NMR structure determination in structural genomics, where the requirement to independently sample many indirect dimensions in a large number of NMR experiments may prevent one from accurately adjusting NMR measurement times to spectrometer sensitivity.

Introduction

NMR-based high-throughput protein structure determination in structural genomics (e.g. Montelione et al., 2000; Yee et al., 2002) is based on triple resonance (TR) NMR experiments (Montelione and Wagner, 1989; Ikura et al., 1990) acquired with $^{13}C/^{15}N$ doubly labeled samples; unlabeled and ^{15}N-labeled proteins are generated primarily for biophysical characterization and to screen for 'foldedness' using 2D $[^{15}N,^{1}H]$-HSQC. Hence, TR NMR data for resonance assignment combined with $^{13}C/^{15}N$ resolved NOESY data constitute the NMR spectroscopic 'backbone' of a structural genomics pipeline. Moreover, (semi-)automated analysis of the NMR spectra (Buchler et al., 1997; Zimmerman et al., 1997; Szyperski et al., 1998; Moseley et al., 2001) is key for high-throughput spectral analysis and requires recording of a redundant set of spectra each affording good spectral resolution. 'Sampling limited' and 'sensitivity limited' data collection regimes have been recently defined (Szyperski et al., 2002), depending on whether the sampling of the indirect dimensions or the sensitivity of the multidimensional NMR experiments *per se* determine the minimally achievable measurement time. Methods that avoid the sampling limited regime are important for future NMR-based structural genomics. Recording of projected, or reduced-dimensionality (RD), NMR spectra (Szyperski et al., 1993a, b, 1994, 1995, 1996; Brutscher et al., 1994, 1995) offers a

*Current address: Department of Chemistry, University of Houston, Houston, TX, U.S.A.
**To whom correspondence should be addressed. E-mail: carrow@oci.utoronto.ca, szypersk@chem.buffalo.edu

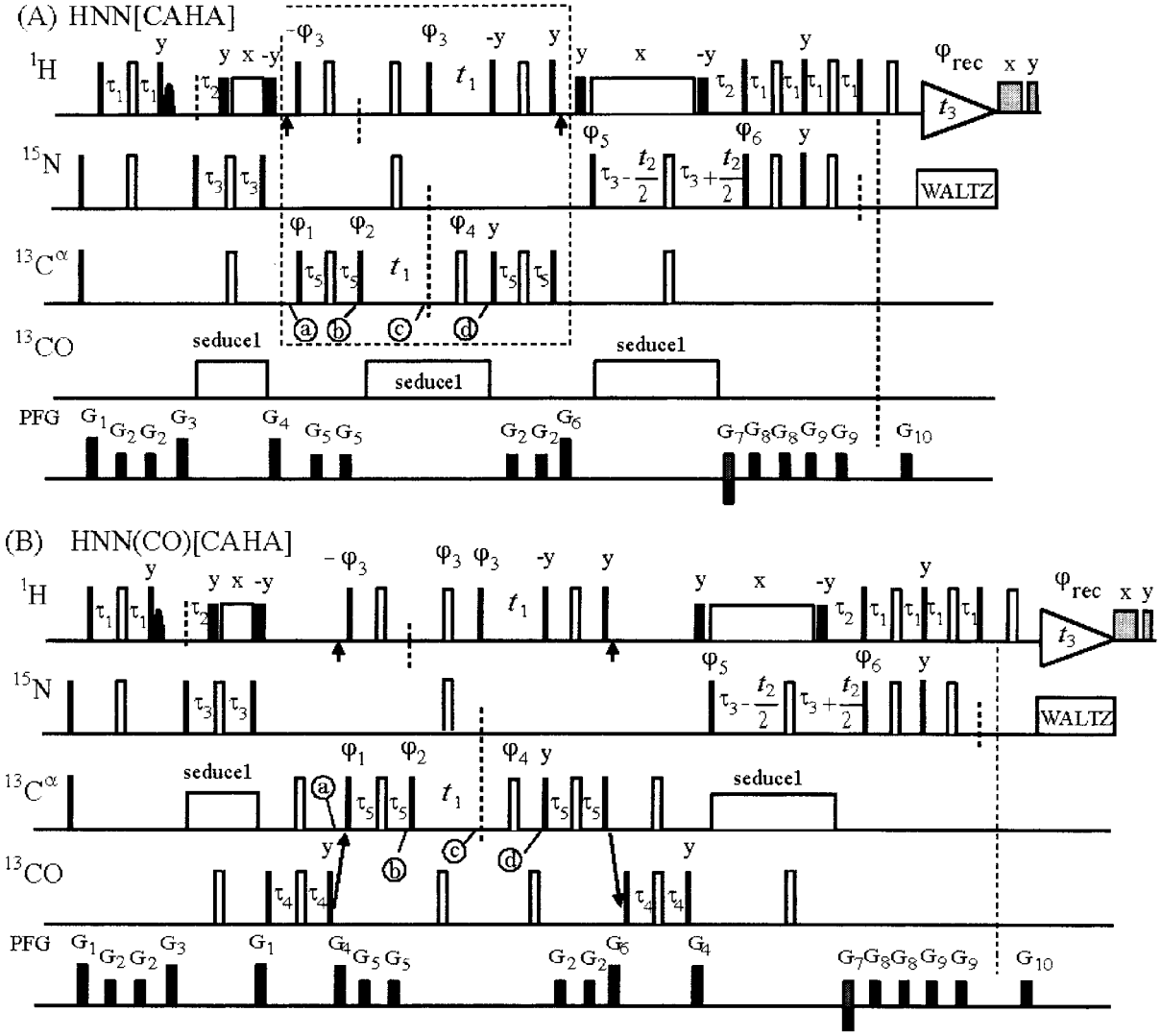

Figure 1. Experimental scheme for the (A) 3D HNN[CAHA] and (B) HNN(CO)[CAHA] experiments. Rectangular 90° and 180° pulses are indicated by filled and open vertical bars or shaped pulses, respectively, and phases are indicated above the pulses. Where no radio-frequency (r.f.) phase is marked, the pulse is applied along x. The simultaneous 180° pulses for $^{13}C^{\alpha}$ and ^{13}CO are effectively realized using a broadband inversion composite pulse consisting of six pulses (Shaka, 1985). The selective 90° pulse on ^{1}H is used to flip back water magnetization along the z-axis (Grzesiek and Bax, 1993) and is applied with profile of a sinc center lobe. The lengths of the rectangular 90° and 180° pulses for $^{13}C^{\alpha}$ are 64.8 μs and 58.6 μs, respectively, and those of the rectangular 90° and 180° pulses for ^{13}CO are 106.6 μs and 123.8 μs, respectively. The ^{1}H and ^{15}N r.f. carrier frequencies were set to 4.75 ppm (to 0 ppm during $^{1}H^{\alpha}$ frequency-labeling in t_1; the vertical arrows indicate the switches of the ^{1}H carrier frequency) and 119 ppm, respectively, and the $^{13}C^{\alpha}$ and $^{13}C'$ r.f. carrier frequencies are chosen to be 56 and 174 ppm. Arrows indicate the change of the carrier frequency on the ^{13}C channel. The spin-lock purge pulses are applied with 15 kHz and are of 8 ms and 3 ms duration, respectively. The delays are: $\tau_1 = 4.6$ ms, $\tau_2 = 5.4$ ms, $\tau_3 = 12$ ms for (A) and 14 ms for (B), $\tau_4 = 4.5$ ms, $\tau_5 = 0.8$ ms. Cosine-modulated seduce1 decoupling (McCoy and Mueller, 1992a) is used for homonuclear ^{13}C decoupling. The durations and strengths of the pulsed z-field gradients (PFGs) are: G1 (500 μs, 30 G/cm); G2 (125 μs, 5 G/cm); G3 (2 ms, 13 G/cm); G4 (500 μs, 15 G/cm); G5 (500 μs, 10 G/cm); G6 (1 ms, 5 G/cm); G7 (1.25 ms, 30 G/cm); G8 (300 μs, 5 G/cm); G9 (200 μs, 10 G/cm); G10 (125 μs, 29.5 G/cm). All PFG pulses are of rectangular shape. A recovery delay of at least 100 μs duration is inserted between a PFG pulse and an r.f. pulse. Phase cycling: $\varphi_1 = (x, -x)$; $\varphi_2 = (y, y, -y, -y)$; $\varphi_3 = (y, y, -y, -y)$; $\varphi_4 = 4(x), 4(-x)$; $\varphi_5 = (x)$; $\varphi_6 = (x)$; $\varphi_{rec} = (x, -x)$. Quadrature detection in t_1 is accomplished by decrementing the phases φ_1, φ_2 and φ_3 according to States-TPPI (Marion et al., 1989). The sensitivity enhancement scheme of Kay et al. (1993) is employed, i.e., the sign of G_7 is inverted in concert with a 180° shift of φ_6.

viable strategy to achieve this goal (Szyperski et al., 2002).

RD NMR experiments afford simultaneous frequency labeling of two spin types in a single indirect dimension, thus effectively projecting an n dimensional on an n−1 dimensional spectrum. The chemical shifts of the projected dimension generate a cosine-modulation of the transfer amplitude, yielding peak doublets encoding n chemical shifts in an n−1 dimensional spectrum. Thus, 4D information can be obtained in a three-dimensional (3D) experiment within a few hours while retaining the resolution routinely achieved in conventional 3D NMR spectra.

Glycine residues represent a particular challenge for accurate automated assignment since they do not provide $^{13}C^{\beta}$ chemical shifts, which generally exhibit a good dispersion and are critical for the automated sequential assignment. Here we present a novel suite of four projected TR NMR experiments which recruit up to four chemical shifts of a single glycine residue (i.e., the $^{13}C^{\alpha}$, $^{1}H^{\alpha 1}$, $^{1}H^{\alpha 2}$ and $^{13}C'$ shifts) for sequential assignment of medium sized proteins (currently smaller than about 20 kDa). Moreover, we introduce a novel type of projection for multidimensional NMR spectra which is distinctly different from the previously published RD NMR approach and belongs to the broader class of simultaneously acquired NMR spectra (Boelens et al., 1994; Pascal et al., 1994; Mariani et al., 1994; Pang et al., 1998; Hu et al., 2001). Its value is demonstrated for the implementation of 3D HNN[CAHA] and HNN(CO)[CAHA] in which the $^{13}C^{\alpha}$ and $^{1}H^{\alpha}$ chemical shifts evolve simultaneously (the corresponding letters in the names of the experiments are given in brackets). These two experiments were complemented by new implementations of RD 3D HNNCOCA and HNNCACO, where $^{13}C'$ and $^{13}C^{\alpha}$ are observed in a common dimension (the corresponding letters in the names of the experiments are underlined). Spectra were acquired for the 10.5 kDa protein TM1112 from the protein structure production pipeline of the Northeast Structural Genomics Consortium (http://www.nesg.org).

Methods

3D HNN[CAHA] and HNN(CO)[CAHA]

The 3D HNN[CAHA] and HNN(CO)[CAHA] experiments correlate the backbone amide ^{15}N and ^{1}HN chemical shifts of residue i with the $^{13}C^{\alpha}$ and $^{1}H^{\alpha}$ chemical shifts of residue i and i−1, respectively, via one-bond scalar couplings. In addition, the two-bond scalar coupling between the $^{15}N_i$ and $^{13}C^{\alpha}_{i-1}$ yields sequential connectivities in 3D HNN[CAHA]. The radio-frequency (r.f.) pulse schemes depicted in Figure 1 were designed to induce an out-and-back type magnetization transfer starting with backbone amide proton magnetization (e.g., Cavanagh et al., 1996). Such transfers have been amply described in the literature (e.g., Szyperski et al., 1998). Thus, we focus on the new r.f. pulse module (boxed in Figure 1) enabling simultaneous quadrature detection of both the $^{1}H^{\alpha}$ and the $^{13}C^{\alpha}$ chemical shift evolution. The use of the same magnetization transfer module in HNN[CAHA] / HNN(CO)[CAHA] ensures that identical line-shapes are obtained in the two experiments along $\omega_1(^{13}C/^{1}H)$.

For employment of the product operator formalism (Sørensen et al., 1983) the spin operators are N_i for the nitrogen of residue i, $^{15}N_i$, C^{α}_i for $^{13}C^{\alpha}_i$, C^{α}_{i-1} for $^{13}C^{\alpha}_{i-1}$, H^{α}_i for $^{1}H^{\alpha}_i$, and C'_{i-1} for $^{13}CO_{i-1}$, $^{1}J_{CH}$ shall represent the scalar couplings between $^{13}C^{\alpha}$ and $^{1}H^{\alpha}$, and $\Omega(X)$ represents the chemical shift of nucleus X. We start the description at time a (indicated in Figure 1), retaining only (i) terms yielding observable magnetization during the detection period, (ii) terms that arise from one-bond scalar couplings and (iii) trigonometric functions that are relevant for the design of this specific module. In particular, passive $^{13}C^{\alpha}$-$^{13}C^{\beta}$ scalar couplings, which lead to signal attenuation during the delays τ_5 and during t_1 (Figure 1), can be adiabatically decoupled (Matsuo et al., 1996; Szyperski et al., 2002) and are not considered. Moreover, constant multiplicative factors are omitted, yielding for 3D HNN[CAHA]

$$\sigma(a) \sim N_{i,z}C^{\alpha}_{i,z} \tag{1a}$$

and for 3D HNN(CO)[CAHA]

$$\sigma(a) \sim N_{i,z}C'_{i-1,z}C^{\alpha}_{i-1,z} \tag{1b}$$

Since the pulse module alluded to above is identical for HNN[CAHA] and HNN(CO)[CAHA], the following description is restricted to Equation 1a, i.e., HNN[CAHA]. The analogous equations for HNN(CO)[CAHA] are easily obtained. For simplicity, we drop the subscript i and have, with $\varphi_1 = x$ (Figure 1), at time b

$$\sigma(b) \sim N_zC^{\alpha}_y \cos\Lambda + N_zC^{\alpha}_xH^{\alpha}_z \sin\Lambda \tag{2a}$$

where $\Lambda = 2\pi^{1}J_{CH}\tau_5$.

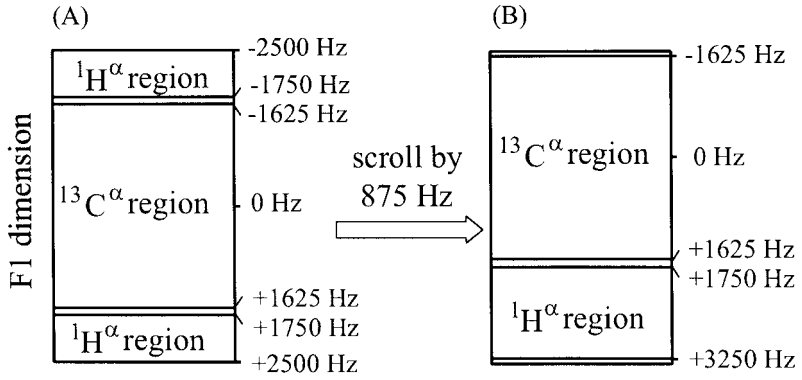

Figure 2. Separation of 'HNNCA-type' and 'HNN(CA)HA-type' peaks in HNN[CAHA] by setting the ^{1}H carrier frequency to 0 ppm and shifting the apparent ^{13}C carrier position by 7 ppm (875 Hz at 500 MHz ^{1}H frequency; see text).

For glycine residues, we have to consider both an active and a passive $^1J_{CH}$ coupling and obtain:

$$\sigma^{Gly}(b) \sim N_z C_y^\alpha \cos^2\Lambda + N_z C_x^\alpha H_z^{\alpha 1} \sin\Lambda\cos\Lambda + N_z C_x^\alpha H_z^{\alpha 2} \sin\Lambda\cos\Lambda + N_z C_y^\alpha H_z^{\alpha 1} H_z^{\alpha 2} \sin^2\Lambda. \quad (2b)$$

The selective 180° pulse on $^{13}C^\alpha$ in the middle of the period $2\tau_5$ decouples the $^{13}C^\alpha$–$^{13}C'$ scalar coupling interaction. With $\varphi_2 = y$ (Figure 1), the next 90° pulse on $^{13}C^\alpha$ generates heteronuclear three-spin order. Hence, in the subsequent evolution period t_1 only the part of the $^{13}C^\alpha$ magnetization that stayed in-phase relative to the attached protons during $2\tau_5$ is frequency-labeled with $\Omega(^{13}C^\alpha)$:

$$\sigma(c) \sim N_z C_y^\alpha \cos\Lambda \mathbf{cos}[\boldsymbol{\Omega}(\mathbf{^{13}C^\alpha})\mathbf{t_1}] + N_z C_z^\alpha H_z^\alpha \sin\Lambda. \quad (3a)$$

For glycines, the term $N_z C_y^\alpha H_z^{\alpha 1} H_z^{\alpha 2}$ is likewise frequency-labeled with $\Omega(^{13}C^\alpha)$:

$$\sigma^{Gly}(c) \sim N_z C_y^\alpha \cos^2\Lambda \mathbf{cos}[\boldsymbol{\Omega}(\mathbf{^{13}C^\alpha})\mathbf{t_1}] + N_z C_z^\alpha H_z^{\alpha 1} \sin\Lambda\cos\Lambda + N_z C_z^\alpha H_z^{\alpha 2} \sin\Lambda\cos\Lambda + N_z C_y^\alpha H_z^{\alpha 1} H_z^{\alpha 2} \sin^2\Lambda \mathbf{cos}[\boldsymbol{\Omega}(\mathbf{^{13}C^\alpha})\mathbf{t_1}]. \quad (3b)$$

Subsequently, transverse $^1H^\alpha$ anti-phase magnetization is generated ($\varphi_3 = y$; Figure 1) which evolves during the second evolution period t_1 with $\Omega(^1H^\alpha)$. The chemical shift evolution of $^{13}C^\alpha$ as well as the one bond $^1H^\alpha$–$^{13}C^\alpha$ scalar coupling are refocussed. We thus have at time d:

$$\sigma(d) \sim N_z C_y^\alpha \cos\Lambda \cos[\Omega(^{13}C^\alpha)t_1] + N_z C_z^\alpha H_x^\alpha \sin\Lambda \mathbf{cos}[\boldsymbol{\Omega}(\mathbf{^1H^\alpha})\mathbf{t_1}], \quad (4a)$$

and

$$\sigma^{Gly}(d) \sim N_z C_y^\alpha \cos^2\Lambda \cos[\Omega(^{13}C^\alpha)t_1] + N_z C_z^\alpha H_x^{\alpha 1} \sin\Lambda\cos\Lambda \mathbf{cos}[\boldsymbol{\Omega}(\mathbf{^1H^{\alpha 1}})\mathbf{t_1}] + N_z C_z^\alpha H_x^{\alpha 2} \sin\Lambda\cos\Lambda \cos[\boldsymbol{\Omega}(\mathbf{^1H^{\alpha 2}})\mathbf{t_1}] + N_z C_y^\alpha H_x^{\alpha 1} H_x^{\alpha 2} \sin^2\Lambda \cos[\Omega(^{13}C^\alpha)t_1] \mathbf{cos}[\boldsymbol{\Omega}(\mathbf{^1H^{\alpha 1}})\mathbf{t_1}] \cos[\Omega(\mathbf{^1H^{\alpha 2}})\mathbf{t_1}]. \quad (4b)$$

Finally, the polarization is transferred back to the amide proton so that the density matrix at the beginning of the detection period is proportional to:

$$\sigma(t_3 = 0) \sim \{\cos^2\Lambda \cos[\Omega(^{13}C^\alpha)t_1] + \sin^2\Lambda \cos[\Omega(^1H^\alpha)t_1]\} \exp[i\Omega(^{15}N)t_2] \quad (5a)$$

and

$$\sigma^{Gly}(t_3 = 0) \sim \{\cos^4\Lambda \cos[\Omega(^{13}C^\alpha)t_1] + \sin^2\Lambda\cos^2\Lambda \cos[\Omega(^1H^{\alpha 1})t_1] + \sin^2\Lambda\cos^2\Lambda \cos[\Omega(^1H^{\alpha 2})t_1] + \sin^4\Lambda \cos[\Omega(^{13}C^\alpha)t_1] \cos[\Omega(^1H^{\alpha 1})t_1] \cos[\Omega(^1H^{\alpha 2})t_1]\} \exp[i\Omega(^{15}N)t_2] \quad (5b)$$

Due to the cosine modulation with three chemical shifts, the last term of Equation 5b yields peaks with fourfold reduced intensity. Hence, these peaks are quite often not observed.

Importantly, the design of the pulse scheme allows one to accomplish quadrature detection along $\omega_1(^{13}C/^1H)$ in a straightforward fashion by decrementing the phases φ_1, φ_2 and φ_3 (Figure 1) according to States-TPPI (Marion et al., 1989); a 90° shift of these phases yields the required imaginary component in which the chemical shift evolution is sine modulated. The new projection technique described here for HNN[CAHA] can likewise be applied to other NMR experiments.

For HNN[CAHA], the first and second term in Equation 5a yield peaks that are equally observed

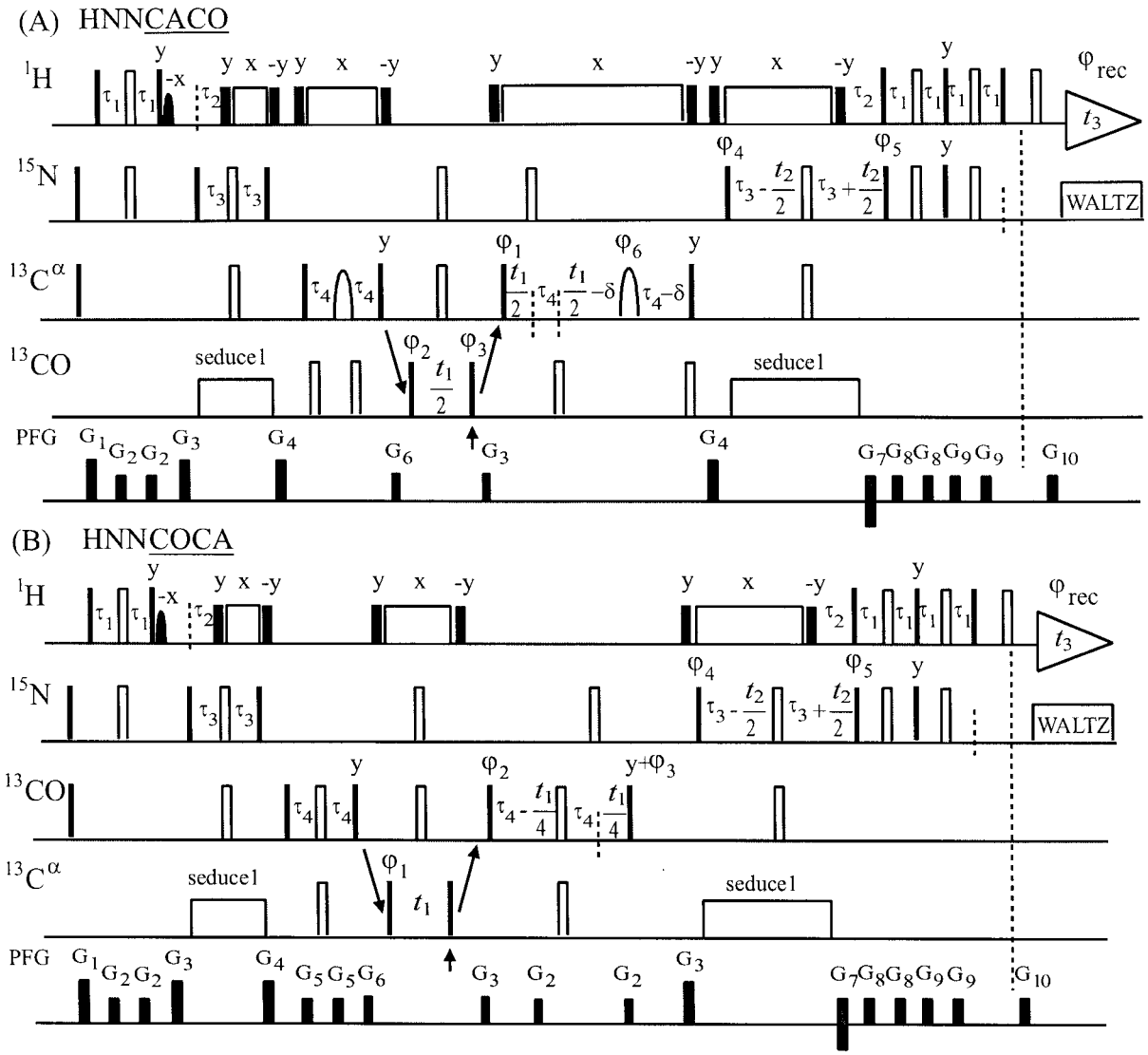

Figure 3. Experimental schemes of (A) 3D HNNCACO and (B) HNNCOCA. The shaped $^{13}C^{\alpha}$ refocusing pulses have the REBURP profile (Geen and Freeman, 1991) and are of 1.6 ms duration (adjusted for a ^{1}H resonance frequency of 500 MHz spectrometer). $\delta = i * (\tau_4 - 0.3\ \text{ms})/(n-1)$, where i and n are the increment index and its maximum value of paired free induction decays in the t_1 dimension. Phase cycling: φ_1 = (x, x, −x, −x); φ_2 = (x, −x); φ_3 is incremented in 309.6° steps according to TPPI in order to shift the apparent carrier position to 160 ppm; φ_4 = (x); φ_5 = (x); φ_6 = (x, x, x, x, −x, −x, −x, −x); φ_{rec} = (x, −x, −x, x). The phases of the pulses indicated with vertical arrows were adjusted to compensate for non-resonance effects (McCoy and Mueller, 1992a, b): the phase shifts are 52° for (A) and 336° for (B), respectively. Quadrature detection in t_1 is accomplished by altering φ_1 by 90° according to States-TPPI (Marion et al., 1989). The sensitivity enhancement scheme of Kay et al. (1993) is employed, i.e., the sign of G_7 is inverted in concert with a 180° shift of φ_5. For other parameters see legend of Figure 1.

in conventional 3D HNNCA and HNN(CA)HA, respectively. To ensure proper detection of the glycine signals in HNNCAHA, the delay $2\tau_5$ must be set to a compromise value around $1/(4\ ^{1}J_{CH})$ (e.g., see Figure 3 in Szyperski et al., 1998). Neglecting relaxation, the 'HNNCA-type' and 'HNN(CA)HA-type' peaks are then equally strong. In parent 4D HNNCAHA (Boucher et al., 1992), the first term in Equations 5a and 5b gives rise to axial magnetization, which is eliminated by application of phase cycling or pulsed field gradients. When acquiring projected NMR spectra, however, this term can be used constructively (Szyperski et al., 1996): in RD NMR, peaks located at the center of peak pairs are observed, while in the novel

implementation presented here the 'HNNCA-peak' is obtained. Hence, when optimizing for co-detection of glycines, the HNNCA information is obtained 'for free' in the projected experiments. The doubling of the t_1-evolution period leads to somewhat broader 'HNNCA-type' peaks in 3D HNN[CAHA] when compared with conventional 3D HNNCA. In contrast, the 'HNN(CA)HA-type' peaks arise from ^{1}H magnetization being transverse solely during the second t_1-evolution period. Thus, these peaks are as strong as if detected in conventional 3D HNN(CA)HA. For larger systems, it might be preferable to transform $N_z C_y^\alpha$ (Equation 3a) into $N_z C_z^\alpha$, while generating two-spin coherence $N_z C_y^\alpha H_x^\alpha$ for frequency labeling with $\Omega(^1H^\alpha)$. This could be achieved by applying a 90°_x pulse on $^{13}C^\alpha$ concomitantly with the 90° pulse on $^1H^\alpha$ with phase φ_3, and by shifting the phase of the last pulse on $^{13}C^\alpha$ by 90°. The presence of transverse magnetization would then be restricted to a single t_1 evolution period for both HNNCA-type and HNN(CA)HA-type peaks.

In order to place the 'HNNCA-type' and 'HNN (CA) HA-type' peaks in separate spectral regions along $\omega_1(^{13}C/^1H)$ (Figure 2), the ^{1}H r.f. carrier frequency is shifted upfield to 0 ppm for $^1H^\alpha$ chemical shift evolution (indicated by vertical arrows in Figure 1), while the ^{13}C carrier is placed as usual at 56 ppm. Since the $^1H^\alpha$ and $^{13}C^\alpha$ chemical shifts range from 3.5 ppm to 6.5 ppm, and from 43 ppm to 71 ppm, respectively, we obtain that the HNN(CA)HA-type and HNNCA-type peaks are located, respectively, in the range from +1750 Hz to +3250 Hz and from −1625 Hz to +1625 Hz at 500 MHz ^{1}H resonance frequency. To ensure that the spectral width in $\omega_1(^{13}C/^1H)$ does not exceed the sum of the spectral widths of $\omega_1(^{13}C)$ in HNNCA and $\omega_1(^1H^\alpha)$ in HNN(CA)HA (i.e., ∼ 5000 Hz at 500 MHz ^{1}H resonance frequency), the resonances between +2500 Hz and +3250 Hz are folded back to the region between −2500 Hz and −1750 Hz. After data acquisition, the apparent carrier position is shifted by 875 Hz (7 ppm on the ^{13}C chemical shift scale) so that the resulting spectrum can be handled like two separate conventional ones (Figure 2).

3D HNNCACO and HNNCOCA

The RD 3D HNNCACO and HNNCOCA experiments correlate the backbone amide ^{15}N and ^{1}HN chemical shifts of residue i with the $^{13}C^\alpha$ and $^{13}C'$ chemical shifts of residue i and i−1, respectively, via one-bond scalar couplings. In addition, the two-bond scalar coupling between the $^{15}N_i$ and $^{13}C^\alpha_{i-1}$ yields sequential connectivities in 3D HNNCACO. The radio-frequency (r.f.) pulse schemes depicted in Figure 3 are designed in an out-and-back fashion, and product operator descriptions of these experiments have been published (Clubb et al., 1992; Cavanagh et al., 1996). The magnetization transfer pathways can be summarized in a short notation as

$$\text{HNNCACO}: {}^1HN_i \rightarrow {}^{15}N_i \rightarrow {}^{13}C_i^\alpha \rightarrow {}^{13}C_i' \searrow {}^{13}C_{i-1}^\alpha \rightarrow {}^{13}C_{i-1}'$$

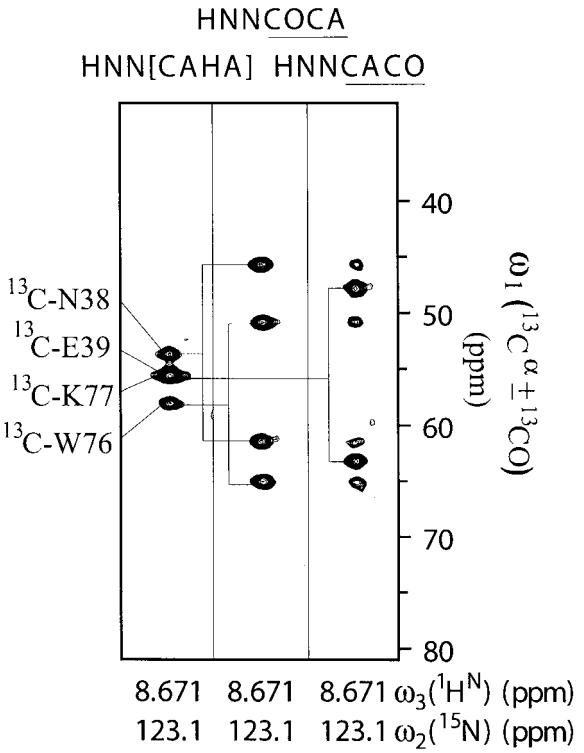

Figure 4. Contour plot of $[\omega_1(^{13}C/^1H), \omega_3(^1H^N)]$-strips taken from HNN[CAHA], 3D HNNCOCA and HNNCACO spectra recorded with a 1 mM sample of the protein TM1112 in 90% H_2O/10% D_2O (pH = 6.5, T = 25 °C, 450 mM NaCl, 25 mM Na_2HPO_4). The strips were taken at the degenerate ^{15}N chemical shifts of the residues 39 and 77, and are centered about their likewise degenerate $^1H^N$ chemical shifts. This chemical shift degeneracy is resolved in conjunction with the RD NMR spectra. The 'HNNCA-type' peaks of HNN[CAHA] define the centers of the peak pairs observed in HNNCOCA and HNNCACO. The spectra were acquired with $70(t_1)*30(t_2)*512(t_3)$ complex points and $t_{1\,max}(^{13}C^\alpha/^{13}C') = 11.2$ ms; $t_{2\,max}(^{15}N) = 22.5$ ms; $t_{3\,max}(^1H^N) = 73.6$ ms. The measurement time was 5.5 and 22 h for 3D HNNCOCA and HNNCACO, respectively. The acquisition parameters for 3D HNN[CAHA] are given in the legend of Figure 7. ^{1}H and ^{13}C chemical shifts are in ppm relative to 2,2-dimethyl-2-silapentane-5-sulfonate sodium salt (DSS).

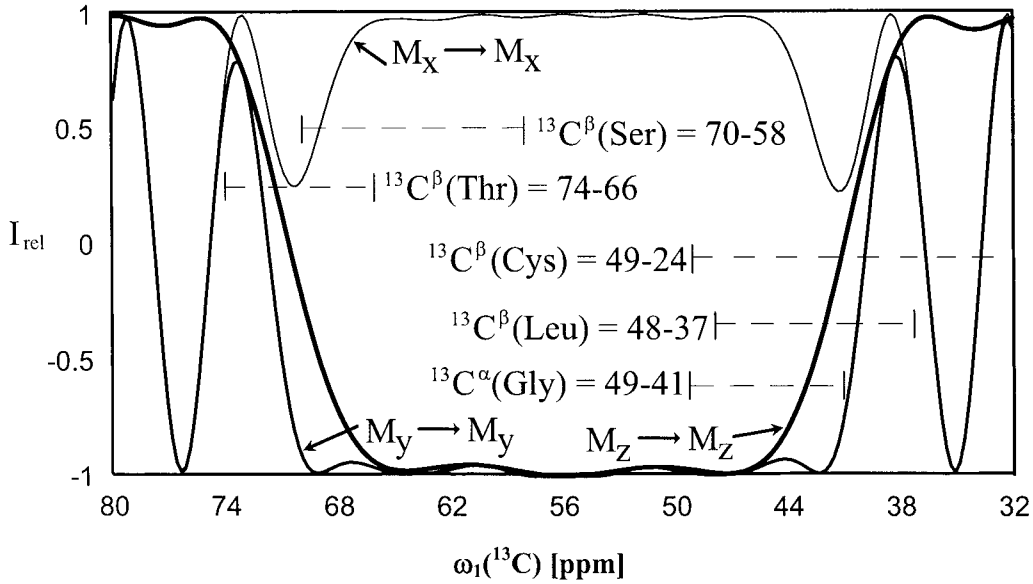

Figure 5. Excitation profile of a 1.6 ms REBURP pulse (Geen and Freeman, 1991) optimized for $^{13}C^{\alpha}$ chemical shift refocussing and $^{13}C^{\alpha}$–$^{13}C^{\beta}$ decoupling during the $^{13}C^{\alpha}$–$^{13}C'$ magnetization transfer in 3D HNNCACO at a ^{1}H resonance frequency of 500 MHz. The phase of the pulse was set to x, and the magnetization at the start of the pulse was set to either M_x, M_y or M_z. The time evolution of the magnetization during the pulse was simulated using the Bloch equations, yielding the fraction of spin-locked magnetization ('$M_x \rightarrow M_x$'), inverted transverse magnetization ('$M_y \rightarrow M_y$') and inverted longitudinal magnetization ('$M_z \rightarrow M_z$'). The ('$M_x \rightarrow M_x$') and ('$M_y \rightarrow M_y$') curves demonstrate that the REBURP pulse is efficiently refocussing the $^{13}C^{\alpha}$ chemical shift in the range from 43.2 to 69.2 ppm (at 500 MHz) which includes all glycine residues (chemical shift range: 41–49 ppm; BioMagResBank, 2002). The chemical shift ranges of the $^{13}C^{\beta}$ resonances of the other residues (horizontal lines) indicate that $^{13}C^{\alpha}$-$^{13}C^{\beta}$ decoupling cannot be achieved for Ser, and may be incomplete for residues such as threonine, leucine and cysteine.

HNNCOCA: $^{1}HN_i \rightarrow ^{15}N_i \rightarrow ^{13}C'_{i-1} \rightarrow ^{13}C^{\alpha}_{i-1}$.

In HNNCACO (Figure 4), REBURP pulses (Geen and Freeman, 1991) were used to refocus the $^{13}C^{\alpha}$ chemical shift and to decouple the $^{13}C^{\alpha}$-$^{13}C^{\beta}$ scalar coupling (e.g., Matsuo et al., 1996) during the heteronuclear magnetization transfer. To ensure that the signals arising from glycine residues are not attenuated due to incomplete refocussing of the $^{13}C^{\alpha}$ chemical shift, the pulse width of these pulses needs to be chosen with care (Yang and Kay, 1999). Figure 5 displays the inversion profile of the REBURP pulse used for the present study, demonstrating that the $^{13}C^{\alpha}$–$^{13}C^{\beta}$ scalar coupling of all serine, most threonine and some cysteine and leucine residues is not refocussed with this approach.

Axial coherences, arising from either incomplete INEPT or steady-state ^{13}C magnetization, can be constructively used to detect peaks located at the center of the peak pairs arising from the cosine modulation of the transfer amplitude with a chemical shift (Szyperski et al., 1996). This allows the unambiguous assignment of multiple peak pairs with identical signal intensities and degenerate chemical shifts in the other dimensions (Szyperski et al., 2002). Such central peak detection is in principle required if $^{15}N/^{1}HN$ chemical shift degeneracy occurs (Szyperski et al., 1996), although in most cases the inspection of the intensities unambiguously reveals which peaks form a pair (Szyperski et al., 2002; Figure 6). For HNNCACO and HNNCOCA, we decided to detect the $^{13}C^{\alpha}$ chemical shift in quadrature and to encode the $^{13}C'$ chemical shift in the in-phase splitting (i.e., to modulate the transfer amplitude with $\cos[\Omega(^{13}C')t_1]$), since the central peaks can be obtained from 3D HNN[CAHA] (the 'HNNCA-type' peaks; Figure 6). To obtain unambiguous assignments, the $^{13}C'$ carrier frequency needs to be shifted to 160 ppm by application of TPPI to the pulse with phase φ_3 in Figure 3A as described (Brutscher et al., 1995; Szyperski et al., 1995). The resulting peak patterns along $\omega_1(^{13}C/^{1}H)$ in HNNCOCA/HNNCACO are shown in Figures 4 and 6.

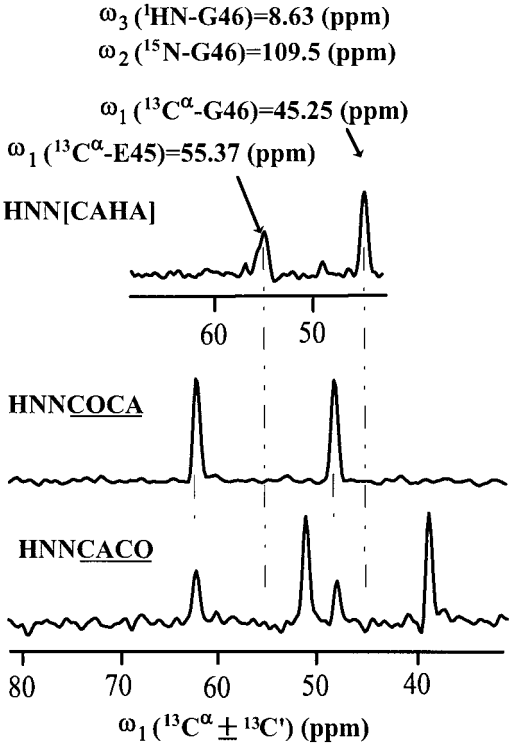

Figure 6. Cross sections taken from 3D HNN[CAHA] (top), 3D HNNCOCA (middle) and 3D HNNCACO (bottom) containing $^{13}C^{\alpha}$ resonances of glycine 46. The 'HNNCA-type' central peaks detected in HNN[CAHA] define the centers of the peak pairs obtained in HNNCOCA and HNNCACO. In HNNCACO, two pairs of peaks emerge reflecting the intra- and interresidue correlation. In principle, the unambiguous identification of the pairs requires the detection of the central peaks, but may also rely on inspection of peak intensities (Szyperski et al., 2002); peaks forming a peak pair arise from a cosine modulation and have (nearly) identical intensity.

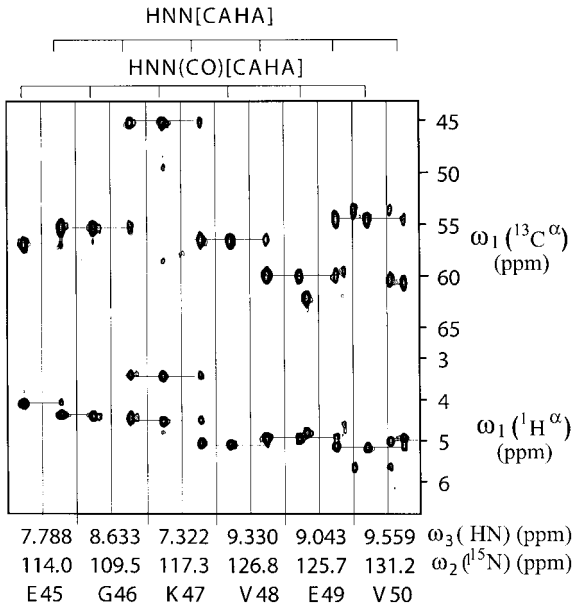

Figure 7. Contour plot of $[\omega_1(^{13}C/^{1}H)$, $\omega_3(^{1}H^{N})]$-strips taken from the 3D HNN[CAHA]/HNN(CO)[CAHA] spectra. The strips were taken at the ^{15}N chemical shifts (indicated at the bottom) of residues 45 to 50. The sequence-specific resonance assignments of the amide chemical shifts are given at the bottom of each strip. The spectra were acquired with $52(t_1) \times 30(t_2) \times 512(t_3)$ complex points and $t_{1,max}(^{13}C^{\alpha}/^{1}H^{\alpha}) = 10.0$ ms, $t_{2,max}(^{15}N) = 20.0$ ms and $t_{3,max}(^{1}H^{N}) = 64$ ms. Eight scans per increment were recorded, resulting in a measurement time of 16.5 h for each spectrum. ^{1}H and ^{13}C chemical shifts are in ppm relative to 2,2-dimethyl-2-silapentane-5-sulfonate sodium salt (DSS).

Results and discussion

The suite of 3D HNNCACO/HNNCOCA (Figure 6), and HNN[CAHA]/HNN(CO)[CAHA] (Figure 7) spectra (Figures 4 and 8) was acquired in 60.5 h for a 1 mM solution (pH = 6.5, 450 mM NaCl, 10 mM DTT, 20 mM Zn^{2+}, 0.01% NaN_3, 95% H2O/5% D_2O) of the 10.5 kDa protein TM1112 on a VARIAN INOVA 500 spectrometer at 25 °C. At this temperature, the protein's overall rotational correlation time obtained from polypeptide backbone ^{15}N $T_{1\rho}/T_1$ ratios (Kay et al., 1989; Szyperski et al., 1993c; Zhu et al., 2000) is about 8.5 ns. The spectra turned out to be of high value to rapidly assign the protein backbone resonances. Firstly, the yield of peak detection, i.e., the ratio of observed peaks over the total number of expected peaks, was very high in all cases: 3D HNN[CAHA] (intraresidue correlations: 100%; interresidue correlations: 99%), HNN(CO)[CAHA] (100%), HNNCACO (intraresidue correlations: 96%; interresidue correlations: 93%) and HNNCOCA (100%). Secondly, three or even four chemical shifts (i.e., the $^{13}C^{\alpha}$, $^{1}H^{\alpha 1}$, $^{1}H^{\alpha 2}$ and $^{13}C'$ shifts) were used to sequentially assign the glycine residues (as shown in Figures 7 and 8 for glycine 46).

In this publication we propose to combine HNN[CAHA]/HNN(CO)[CAHA] and RD HNNCACO/HNNCOCA. HNN[CAHA]/HNN(CO)[CAHA] are obtained with a novel acquisition scheme that enables simultaneous acquisition of two spectra originating from either the in-phase or the anti-phase component(s) present whenever an INEPT step remains incomplete. The simultaneous acquisition of NMR spectra has been realized for several TR (Boelens et al., 1994; Mariani et al., 1994; Pang et al., 1998; Hu et al., 2001) and heteronuclear resolved NOESY (Pascal et al., 1994) experiments. To the best of our knowledge, however, only independent coherence transfer pathways have been used. In these cases,

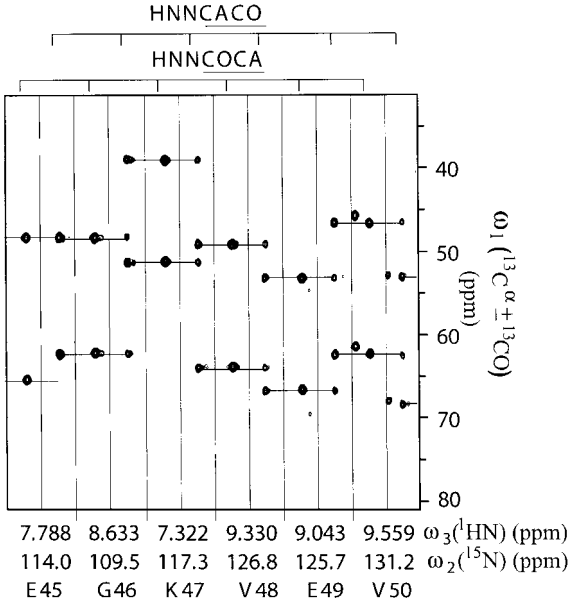

Figure 8. Contour plot of [$\omega_1(^{13}C/^1H)$, $\omega_3(^1H^N)$]-strips taken from the 3D HNNCOCA/HNNCACO spectra. The strips were taken at the ^{15}N chemical shifts (indicated at the bottom) of residues 45 to 50. The sequence-specific resonance assignments of the amide chemical shifts are given at the bottom of each strip. The acquisition parameters of these spectra are given in the legend of Figure 4.

the required simultaneous quadrature detection does not represent a particular challenge for pulse sequence design. An obvious advantage of simultaneous acquisition of NMR spectra is due to the fact that even small variations of chemical shifts, which may be due to different r.f. duty cycles in different NMR pulse schemes, are avoided. This feature is valuable for automatic resonance assignment protocols where tolerances for chemical shift measurements are critical parameters for the assignment yield.

The key advantage of the RD NMR approach compared with simultaneous acquisition of spectra is due to the fact that all shift correlations are preserved upon projection. While an RD 3D NMR spectrum with central peak detection is equivalent to a 4D spectrum, two simultaneously acquired 3D spectra are obviously not. On the other hand, the advantages of simultaneous acquisition when compared with RD NMR can be summarized as follows. Firstly, the sensitivity remains to be the one of conventional 3D experiments. Secondly, the spectral width in the projected dimension is moderately reduced. Thirdly, since chemical shifts are detected as single-quantum coherences, computer support to obtain the shifts is less critical (e.g., Szyperski et al., 1998). Overall, the combined use of RD NMR and simultaneous data acquisition approaches promises to be a valuable extension for future high-throughput protein assignment efforts.

Among the four experiments proposed here, 3D HNNCACO is the least sensitive one. In fact, the successful use of the HNNCACO/HNNCOCA approach for larger systems has been shown to crucially depend on protein deuteration (Yamazaki et al., 1994; Konrat et al., 1999). Moreover, the value of recording a 4D version of the 3D HNN<CA,CO> experiment (Szyperski et al., 1995), in which the backbone amide ^{15}N and ^1HN chemical shifts of residue i are correlated with the $^{13}C^{\alpha}$ chemical shifts of residue i and the $^{13}C'$ chemical shift of residue i-1, for resolving $^{15}N/^1HN$ chemical shift degeneracy has been demonstrated (Konrat et al., 1999). Hence, 3D HNN<CA,CO> appears to be an attractive choice to complement the suite of four experiments presented here.

Acknowledgements

This work was supported by the *Ontario Research and Development Challenge Fund* (to C.H.A.), the *National Science Foundation* (MCB 0075773 to T.S.) and the *National Institutes of Health* (Northeast Structural Genomics Consortium; P50 GM62413-01 to T.S. and C.H.A.). We thank Dr A. Yee and A. Semesi for helpful discussions.

References

Boelens, R., Burgering, M., Fogh, R.H. and Kaptein, R. (1994) *J. Biomol. NMR,* **4**, 201–213.

Boucher, W., Laue, E.D., Campbell-Burk, S. and Domaille, P.J. (1992a) *J. Am. Chem. Soc.*, **114**, 2262–2264.

Boucher, W., Laue, E.D., Campbell-Burk, S. and Domaille, P.J. (1992b) *J. Biomol. NMR*, **2**, 631–637.

Brutscher, B., Simorre, J.P., Caffrey, M.S. and Marion, D. (1994) *J. Magn. Reson.*, **B105**, 77–82.

Brutscher, B., Cordier, F., Simorre, J.P., Caffrey, M.S. and Marion, D. (1995) *J. Biomol. NMR*, **5**, 202–206.

Buchler, N.E.G., Zuiderweg, E.R.P., Wang, H. and Goldstein, R.A. (1997) *J. Magn. Reson.*, **125**, 34–42.

Cavanagh, J., Fairbrother, W.J., Palmer III, A.G. and Skelton, N.J. (1996) *Protein NMR Spectroscopy*. Wiley, New York.

Clubb, R.T., Thanabal, V. and Wagner, G. (1992) *J. Biomol. NMR*, **2**, 203–210.

Geen, H. and Freeman, R.J. (1991) *J. Magn. Reson.*, **93**, 93–141.

Grzesiek, S. and Bax, A. (1993) *J. Am. Chem. Soc.*, **115**, 12593–12594.

Hu, W.D., Gosser, Y.Q., Xu, W.J. and Patel, D.J. (2001) *J. Biomol. NMR*, **20**, 167–172.

Ikura, M., Kay, L.E. and Bax, A. (1990) *Biochemistry*, **29**, 4659–4667.

Kay, L.E., Keifer, P. and Saarinen, T. (1992) *J. Am. Chem. Soc.*, **114**, 10663–10665.

Kay, L.E., Torchia, D.A. and Bax, A. (1989) *Biochemistry*, **28**, 8972–8979.

Konrat, R., Yang, D. and Kay, L.E. (1999) *J. Biomol. NMR*, **15**, 309–313.

Mariani, M., Tessari, M., Boelens, R., Vis, H. and Kaptein, R. (1994) *J. Magn. Reson.*, **B104**, 294–297.

Marion, D., Ikura, M., Tschudin, R. and Bax, A. (1989) *J. Magn. Reson.*, **85**, 393–399.

Matsuo, H., Kupce, E., Li, H. and Wagner, G. (1996) *J. Magn. Reson.*, **B113**, 91–96.

McCoy, M.A. and Mueller, L. (1992a) *J. Am. Chem. Soc.*, **114**, 2108–2112.

McCoy, M.A. and Mueller, L. (1992b) *J. Magn. Reson.*, **99**, 18–36.

Montelione, G.T. and Wagner, G. (1989) *J. Am. Chem. Soc.*, **111**, 5474–5475.

Montelione, G.T., Zheng, D., Huang, Y., Gunsalus, C. and Szyperski, T. (2000) *Nat. Struct. Biol.*, **7**, 982–984.

Moseley, H.N.M., Tejero, R., Zimmerman, D.E., Celda, B., Nilsson, B. and Montelione, G.T. (2002) *Methods Enzymol.*, **339**, 91–108.

Pang, Y.X., Zeng, L., Kurochkin, A.V. and Zuiderweg, E.R.P. (1998) *J. Biomol. NMR*, **11**, 185–190.

Pascal, S.M., Muhandiram, D.R., Yamazaki, T., Forman-Kay, J.D. and Kay, L.E. (1994) *J. Magn. Reson.*, **103**, 197–201.

Sørensen, O.W., Eich, G.W., Levitt, M.H., Bodenhausen, G. and Ernst, R.R. (1983) *Prog. NMR Spectrosc.*, **16**, 163–192.

Szyperski, T., Wider, G., Bushweller, J.H. and Wüthrich, K. (1993a) *J. Biomol. NMR*, **3**, 127–132.

Szyperski, T., Wider, G., Bushweller, J.H. and Wüthrich, K. (1993b) *J. Am. Chem. Soc.*, **115**, 9307–9308.

Szyperski, T., Luginbühl, P., Otting, G., Güntert, P. and Wüthrich, K. (1993c) *J. Biomol. NMR*, **3**, 151–164.

Szyperski, T., Pellecchia, M. and Wüthrich, K. (1994) *J. Magn. Reson.*, **B105**, 188–191.

Szyperski, T., Braun, D., Fernandez, C., Bartels, C. and Wüthrich, K. (1995) *J. Magn. Reson.*, **B108**, 197–203.

Szyperski, T., Braun, D., Banecki, B. and Wüthrich, K. (1996) *J. Am. Chem. Soc.*, **118**, 8146–8147.

Szyperski, T., Banecki, B., Braun, D. and Glaser, R.W. (1998) *J. Biomol. NMR*, **11**, 387–405.

Szyperski, T., Yeh, D.C., Sukumaran, D.K., Moseley, H.N.B. and Montelione, G.T. (2002) *Proc. Natl. Acad. Sci. USA*, **99**, 8009–8014.

Yamazaki, T., Lee, W., Arrowsmith, C.H., Muhandiram, D.R. and Kay, L.E. (1994) *J. Am. Chem. Soc.*, **116**, 11655–11666.

Yang, D. and Kay, L.E. (1999) *J. Am. Chem. Soc.*, **121**, 2571–2575.

Yee, A., Chang, X., Pineda-Lucena, A., Wu, B., Semesi, A., Le, B., Ramelot, T., Lee, G.M., Bhattacharyya, S., Gutierrez, P., Denisov, A., Lee, C.-H., Cort, J.R., Kozlov, G., Liao, J., Finak, G., Chen, L., Wishart, D., Lee, W., McIntosh, L.P., Gehring, K., Kennedy, M.A., Edwards, A.M. and Arrowsmith, C.H. (2002) *Proc. Natl. Acad. Sci. USA*, **99**, 1825–1830.

Zhu, G., Xia, Y., Nicholson, L.K. and Sze, K.H. (2000) *J. Magn. Reson.*, **143**, 423–426.

Zimmerman, D.E., Kulikowski, C.A., Huang, Y., Feng, W., Tashiro, M., Shimotakahara, A., Chien, C.Y., Powers, R. and Montelione, G.T. (1997) *J. Mol. Biol.*, **269**, 592–610.